An Enhanced Adaptive P&O MPPT for Fast and Efficient Tracking Under Varying Environmental Conditions

Jubaer Ahmed, *Member, IEEE* and Zainal Salam, *Member, IEEE*

***Abstract*—This paper proposes an enhanced adaptive perturb and observe (EA-P&O) maximum power point tracking (MPPT) algorithm for the photovoltaic system. The objective is to mitigate the limitations of the conventional P&O namely, the steady-state oscillation, diverged tracking direction, and inability to detect the global peak during partial shading. A smart oscillation detection scheme and a dynamic boundary condition resolve the first two problems, respectively. Meanwhile, an intelligent prediction method is designed to ensure that the global peak is always correctly tracked. Another feature is the open-circuit voltage is determined without using sensors. The proposed idea is verified using MATLAB simulations by imposing stringent dynamic irradiance and partial shading tests. Moreover, an experimental validation is carried out using a buck–boost converter in conjunction with dSpace DS1104 DSP board. The performance of the algorithm is compared with four prominent MPPT techniques: first, the artificial bee colony; second, modified incremental conduction; third, cuckoo search; and fourth, the hybrid ant colony optimization-P&O. The results show that the proposed method tracks the global peak successfully under distinctive patterns of partial shading, when other algorithms fail occasionally. On top of that, it improves the tracking speed by two to three times, while efficiency is maintained over 99%.**

***Index Terms*—MPPT, PV, solar, P&O, tracking MPP, P-V curve.**

I. Introduction

SOFT computing methods are increasingly utilized to develop MPPT algorithms for photovoltaic (PV) system. This is evident from the recent proliferation of MPPT techniques using particle swarm optimization (PSO) [1], differential evolution (DE) [2], artificial neural network (ANN) [3], ant colony optimization (ACO) [4], artificial bee colony (ABC) [5], grey wolf (GW) [6], fireflies (FF) [7], and cuckoo search (CS) [8] etc. The main advantages of these techniques are their inherent ability to handle challenging environmental scenarios such as partial shading and dynamic irradiance changes. Despite having higher efficiency, it is difficult to overlook the complexity, computational burden, implementation cost and slow tracking speed associated with them [9], [10]. Consequently, in many recent work, conventional MPPT methods such as perturb and observation (P&O) [11]–[13], hill climbing (HC) [14], [15] and incremental conductance (IC) are re-visited and improved.

Among all the conventional MPPT, P&O is the simplest and exhibits very fast convergence towards the maximum power point (MPP). However, it suffers from three serious drawbacks. First, the algorithm continuously oscillates around the MPP. The oscillation is inevitable due to the nature of the algorithm that forces the operating point to move forward and backward around the MPP with respect to the imposed perturbation. Depending on the size of the perturbation, the oscillation results in certain amount of power loss. Second, the P&O is prone to lose its tracking direction when the irradiance increases rapidly with time [16]. Once the tracking direction is incorrect, the algorithm becomes confused and it diverges further away from the MPP. If this happens, the energy loss would be considerable. Third, the P&O—in its original form, is not capable of tracking the global peak under partial shading condition.

A number of researchers have worked on P&O to remove these limitations from different aspects. In [11]–[13], [17], [18], several adaptive versions of the P&O are proposed to reduce the steady state oscillation. Despite the successful implementation of these schemes, the divergence problem for rapidly increasing irradiance remain unsolved. A number of recent work, notably by [14]–[16] dealt with the divergence along with the oscillation issue. The solutions are, nevertheless, case dependent and the algorithms fail to work correctly under different conditions, as highlighted in [19]. Apart from these, the simulation and experiments do not reflect the adverse environmental situations experienced by the PV system in the real world. Based on this concern, a highly effective adaptive P&O that simultaneously address the steady state oscillation and divergence problems in [19]. It detects the oscillation by recording five consecutive perturbation directions and minimizes its amplitude to mitigate the steady state loss. Besides, it applies a dynamic voltage boundary scheme to guide the tracking under ascending irradiance change. However, it is important to note that, the above-mentioned techniques, including [19] do not provide any solution for partial shading conditions.

On the other hand, there are several works that focus on P&O that can deal with partial shading [20]–[22]. However, these works completely ignore the steady state oscillation and

Manuscript received August 10, 2017; revised December 11, 2017; accepted January 1, 2018. Date of publication January 11, 2018; date of current version June 18, 2018. This work was supported by the Ministry of Higher Education, Malaysia, under the Malaysia Rising Star Award Grant. It was managed by Universiti Teknologi Malaysia, under vot. no. R.J130000.7823.4F919. Paper no. TSTE-00731-2017. *(Corresponding author: Zainal Salam.)*

J. Ahmed was with the Centre of Electrical Energy Systems, Faculty of Electrical Engineering, Universiti Teknologi Malaysia, Johor Bahru 81310, Malaysia. He is now with the Faculty of Engineering, Computing and Science, Swinburne University of Technology Sarawak, Kuching 93350, Malaysia (e-mail: jahmed@swinburne.edu.my).

Z. Salam is with the Centre of Electrical Energy Systems, Faculty of Electrical Engineering, and the Institute of Future Energy, Universiti Teknologi Malaysia, Johor Bahru 81310, Malaysia (e-mail: zainals@fke.utm.my).

Color versions of one or more of the figures in this paper are available online at http://ieeexplore.ieee.org.

Digital Object Identifier 10.1109/TSTE.2018.2791968

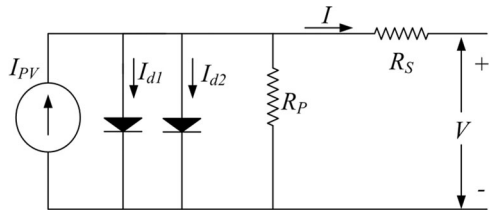

Fig. 1. The two-diode model of solar cells.

divergence problem. Thus, the solutions provided by the previous works do not address all three issues simultaneously.

Recently, there are efforts to combine the P&O with metaheuristic algorithms such as FF, ACO, PSO, GW to track global peak under partial shading. This is known as the hybrid approach [4], [23]–[26]. Unfortunately, by doing so, the P&O losses its simple structure. Furthermore, the computational burden has significantly increased due to the incorporation of metaheuristic algorithms.

Based on the literature survey, there appears to be an absence of a single P&O algorithm that can comprehensively handle all the three limitations. Thus, the objective of this work is to propose an enhanced adaptive P&O (EA-P&O) that minimizes the steady state oscillation and solves the divergence problem by applying a dynamic boundary condition, similar to the work carried out in [19]. In addition, the algorithm detects the partial shading occurrence and perform a rapid search for the global peak. Another important feature is that, the values of open circuit voltage and irradiance are continuously updated without the use of temperature and irradiance sensors respectively. This reduces the cost and complexity of the MPPT implementation considerably.

II. PV Modeling

To date, several PV models are reported in literature; the more popular ones are the single diode model, R_S, R_P and the two-diode model [27]. Its main purpose is to emulate the behavior of PV modules in circuit form, so that it can be integrated into the available electrical-based computational software, such as MATLAB/Simulink. To ensure better accuracy, two diode model is used in this paper as shown in Fig. 1.

If V is the voltage, then the PV current drawn from the system can be written according to two diode models as

$$I = I_{\mathrm{PV}} - I_{d1} - I_{d2} - \frac{V + IR_s}{R_p} \tag{1}$$

where R_s and R_p are the series and parallel resistance, respectively, while V_T is the thermal voltage of the diodes. The light generated current (I_{PV}) is given by

$$I_{\mathrm{PV}} = \left(I_{\mathrm{PV\text{-}STC}} + K_I(T - T_{\mathrm{STC}})\right)\frac{G}{G_{\mathrm{STC}}} \tag{2}$$

Note that I_{PV_STC} is measured in the standard test condition (STC), i.e., temperature $T = 298$ K (25 °C) and irradiance $G = 1000$ W/m^2. Variable K_I is the short circuit current coefficient, which is usually provided by the manufacturer. The diode saturation current is given by [27]

$$I_{d1} = I_{d2} = \frac{I_{\mathrm{SC-STC}} + K_I(T - T_{\mathrm{STC}})}{\exp\left(\left(V_{\mathrm{OC-STC}} + K_V(T - T_{\mathrm{STC}})\right)/\,V_T\right) - 1} \tag{3}$$

TABLE I
THE SPECIFICATIONS OF THE PV MODULE MSX60

Parameters	Label	Value
Short Circuit current	I_{SC}	3.8 A
Open circuit voltage	V_{OC}	21.1 V
Current at Pmax	I_{MPP}	3.5 A
Voltage at Pmax	V_{MPP}	17.1 V
Maximum power	P_{MPP}	59.85 W
V_{OC} coef. of temperature	K_V	−0.08 V°C
I_{SC} coef. of temperature	K_I	3e^{-3} A°C
cell in series per module	n	36

TABLE II
INITIALIZATION PARAMETERS

Parameters	Symbol	Value
Open circuit voltage of a module	V_{OC}	21.1 V
Number of modules in series	N_S	10
Open circuit voltage of PV array	$V_{\mathrm{oc\_array}}$	211 V
Initial perturbation	ΔV	4.22
Initial Voltage of EA-P&O	V_{out}	137.2 V
Steady state flag	steady	0
Oscillation counter	osc	0
Perturbation direction	ϕ	+1
Perturbation counter	slope	[0,0,0,0,0]
Voltage Lower limit	V_{refl}	10.6 V
Voltage Upper limit	V_{refh}	200.6 V

In (3), $I_{\mathrm{SC\_STC}}$ and $V_{\mathrm{OC\_STC}}$ are the short circuit current and the open circuit voltage in STC, respectively. Variable K_V is the temperature coefficient of the voltage. The specifications for the PV module used in this paper are given in Table I.

III. The Enhanced Adaptive P&O (EA-P&O)

A. Initialization

The objective of the EA-P&O is to ensure that steady state oscillation and the deviation from the tracking locus is minimized along with the tracking of the global peak under partial shading. To accomplish that, the complete flowchart is implemented as illustrated in Fig. 2. EA-P&O requires several initialization parameters as given in Table II. To facilitate numerical explanation, data from MSX60 PV module is presented in Table II.

B. Tracking Under Uniform Irradiance

Based on critical observation by numerous researches [20], [21] that the MPP lies in the vicinity of $0.8 \times V_{\mathrm{oc\text{-}array}}$ $(V_{\mathrm{oc\text{-}array}} = V_{\mathrm{oc}} \times N_s)$. It is explained in [19] that, it is appropriate to initialize at $0.65 \times V_{\mathrm{oc\_array\text{-}STC}}$, so that MPPT can record few perturbation directions before converging at MPP. Initial perturbation size is set as $0.02V_{\mathrm{oc\text{-}array}}$.

After initialization, EA-P&O reads voltage (V) and current (I) from PV array and calculates power. Afterwards, a checking is done based on comparing normalized power $(\Delta P/P)$ and $(\Delta \mathrm{V})$ with two thresholds 0.1 and $0.005V_{\mathrm{oc\_array}}$ respectively within the large power deviation box in Fig. 2. However, such checking results is 'no' initially, as $\Delta P/P$ can be more than 0.1 but ΔV will not be less than or equal to $0.005V_{\mathrm{oc\text{-}array}}$ during initial scanning state. Consequently, EA-P&O will shift to flag 0.

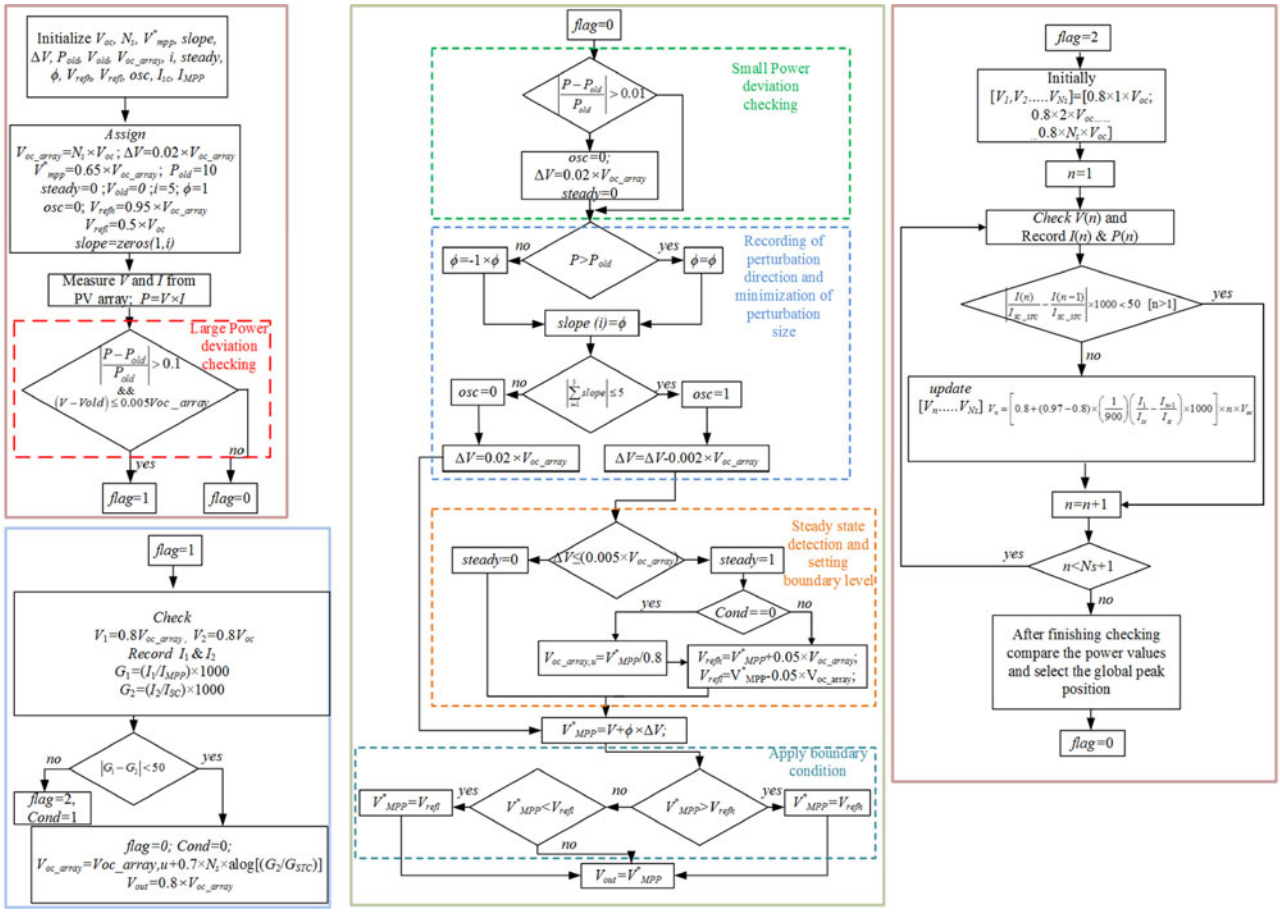

Fig. 2. Comprehensive flowchart for EA-P&O.

Afterward, MPPT requires few samples to reach at MPP. As it reaches there, it starts oscillating around MPP that results to steady state loss. EA-P&O detects such oscillation by recording five consecutive perturbation directions. Then checking condition in (4) is applied for oscillation detection [19].

$$if \sum \text{slope} = \begin{cases} 5 \text{.....[MPPT not converged to steady state]} \\ < 5 \text{.....[MPPT converged to steady state]} \end{cases} \quad (4)$$

When oscillation is detected it minimizes the perturbation size to $0.005V_{\text{oc\_array}}$. Consequently, oscillation is minimized as well as the energy loss. The moment perturbation is reduced to the minimum level, the value of 'steady' is toggled to 1. If under this uniform irradiance condition, voltage of the PV array is expected to be at MPP (V^*_{MPP}) and oscillating with minimum perturbation. It is reported in many researches [28], that in mono and poly crystalline silicon based PV modules MPP occurs approximately at $0.8V_{\text{oc\_array}}$.

Such relation can be used alternatively to update $V_{\text{oc\_array}}$ dynamically as

$$V_{\text{oc\_array},u} = \frac{V^*_{\text{MPP}}}{0.8} \quad (5)$$

Thus, whenever EA-P&O tracks the MPP, it updates $V_{\text{oc\_array}}$ continuously. As a result, the variation of $V_{\text{oc\_array}}$ due to temperature will not affect the performance of MPPT. Besides, no temperature sensors are needed to update $V_{\text{oc\_array}}$ continuously.

After tracking the MPP, EA-P&O imposed a dynamic boundary condition) on operating voltage around the MPP region which restrict the operating point to diverge from the MPP. As presented in (6), upper and lower boundary is set as V_{refh} and V_{refl} respectively around V^*_{MPP} by 5% of the $V_{\text{oc\_array}}$.

$$\begin{aligned} V_{\text{refh}} &= V^*_{\text{MPP}} + 0.05 \times V_{\text{oc\_array}}; \\ V_{\text{refl}} &= V^*_{\text{MPP}} - 0.05 \times \text{V}_{\text{oc\_array}}; \end{aligned} \quad (6)$$

Conventional P&O is prone to diverge from the MPP when G starts ascending gradually with a fast gradient. Such occurrence reduced the efficiency from 10–50% depending on the ramp of G [16]. Imposed boundary condition restrains the operating point being diverged from MPP trail as presented in Fig. 3.

After settling at MPP with restricted voltage boundary, there are possibility of having four different conditions:

a) irradiance will vary (increase or decrease) slowly
b) Temperature will vary
c) sudden large change in irradiance
d) occurrence of partial shading.

During incident (a), if rate of change of irradiance $(\Delta G/\Delta t)$ is less than 10 W/m^2/s, MPPT performance is not affected by divergence problem [19]. However, if $(\Delta G/\Delta t)$ is over 10 W/m^2/s, conventional P&O diverges from the MPP locus that results in significant power loss [29].

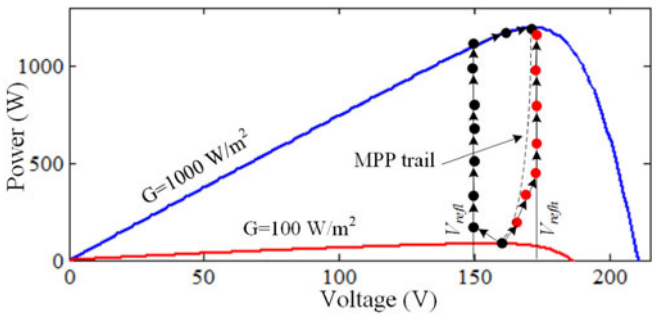

Fig. 3. Restricting operating voltage near MPP.

It is presented mathematically in [19], when G starts changing, the relation between two consecutive samples scanned by MPPT is

$$\frac{\Delta P}{P} = \frac{\Delta G}{G_{\mathrm{STC}}} \tag{7}$$

Thus, if $\Delta G/\Delta t \geq 10\,\mathrm{W/m^2/s}$, the threshold for normalized power can be calculated as $\Delta P/P = \Delta G/G_{\mathrm{STC}} = (10/1000) = 0.01$.

In Fig. 2, inside flag 0 EA-P&O continuously checks for whether $\Delta P/P > 0.01$ or not. If it is bigger than that then, EA-P&O entertain the possibility of occurring irradiance change with high rate. Thus, perturbation size is restored to initial $0.02V_{\mathrm{oc\_array}}$ so that voltage can follow the MPP trail and the variable 'steady' is toggled to 0. Due to large perturbation. voltage starts diverging from MPP trail. However, upper and lower boundary condition force the voltage to remain near the MPP all the time as depicted in Fig. 3. Thus, power loss due divergence issue is mitigated.

In case of temperature change (condition (b)), it is practically a very slow process which takes span of hours. However, $V_{\mathrm{oc\_array}}$ change significantly with temperature. As EA-P&O updates $V_{\mathrm{oc\_array}}$ using (5), temperature change does not affect MPPT performance.

If the condition (c) or (d) takes place, sudden change in irradiance or partial shading can be sensed primarily by a large change in power deviation. It is presented in [30], [31], majority of the MPPT algorithm in literature cannot distinguish between these two conditions. Whenever, they sense a large change in power they initiate global peak searching under partial shading although partial shading may not be present at that time.

In EA-P&O, such sudden power change is detected by large power deviation block. When the condition is satisfied, EA-P&O initiates flag 1. Then, EA-P&O scan two specific voltage on the curve at $V_1 = 0.8V_{\mathrm{oc\_array}}$ and $V_2 = 0.8V_{\mathrm{oc}}$. Here, V_1 and V_2 lies at MPP position and short circuit current position respectively. Thus, recorded current at these two points are I_1 and I_2 represents I_{MPP} and I_{SC}. Afterwards, based on these two-current values irradiance level (G) on the $I-V$ curve can be calculated as follows [30].

At $I_1 = I_{\mathrm{MPP}}$

$$G_1 = \frac{I_{\mathrm{MPP}}}{I_{\mathrm{MPP\_STC}}} \times G_{\mathrm{STC}} \tag{8}$$

At $I_2 = I_{\mathrm{SC}}$

$$G_2 = \frac{I_{\mathrm{SC}}}{I_{\mathrm{SC\_STC}}} \times G_{\mathrm{STC}} \tag{9}$$

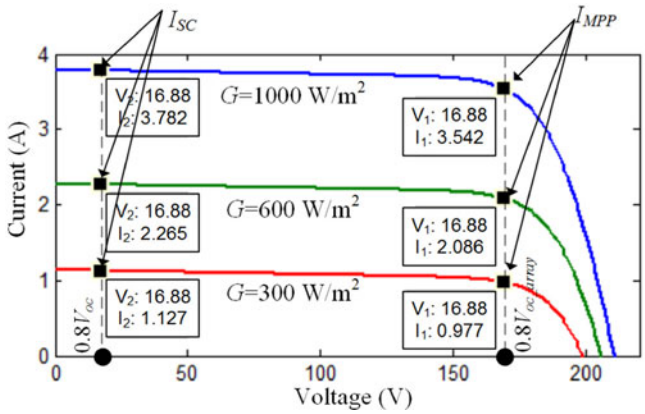

Fig. 4. Characteristics of $I-V$ curve during uniform irradiance.

This proposed scheme can be numerically verified using the following example. In Fig. 4, $I-V$ curve under three irradiance level (1000, 600 and 300 W/m^2) is illustrated. On the curve, respective currents for the $I_{\mathrm{SC}} = I_{0.8Voc}$ and $I_{\mathrm{MPP}} = I_{0.8V\mathrm{oc\_array}}$ are marked. For MSX 60 PV module at STC the I_{SC} is 3.8 A and I_{MPP} is 3.5 A. At 1000 W/m^2, using (8) & (9) the G_1 and G_2 can be calculated as follows.

At I_{MPP}

$$G_1 = \frac{I_{\mathrm{MPP}}}{I_{\mathrm{MPP\_STC}}} \times G_{\mathrm{STC}} = \frac{3.542}{3.5} \times 1000 = 1012$$

At I_{SC}

$$G_2 = \frac{I_{\mathrm{SC}}}{I_{\mathrm{SC\_STC}}} \times G_{\mathrm{STC}} = \frac{3.782}{3.8} \times 1000 = 995.3$$

It can be seen that the calculated values of G_1 and G_2 are very close to the actual 1000 W/m^2. However, values differ by 17.

Similarly using the $I-V$ curve for 600 W/m^2, the values of G_1 and G_2 is 596 W/m^2, thus having no mismatch. However, it is noticeable that, at 300 W/m^2 the calculated value for G_1 is 296 W/m^2 but G_2 is 279 W/m^2 which has a discrepancy of 17. Based on these observations, an important deduction can be made: once G_1 and G_2 is calculated and mismatch remains below a certain threshold, the algorithm treats the condition as a uniform irradiance.

It is reported in [30] that, in mono and poly crystalline based PV modules the absolute difference between G_1 and G_2 always remain less than 40 under uniform irradiance. Thus, under flag 1 in Fig. 2, a checking is done to find the difference between G_1 and G_2. Though instead of 40, threshold is set to 50 to have a margin of safety. If a large power deviation is due to large change of uniform irradiance, then $|G_1 - G_2|$ will remain below 50, otherwise it will be considered as a partial shading case.

If it is a case of large uniform irradiance change, there is no need to go for partial shading scanning. Instead of that, EA-P&O re-calculate $V_{\mathrm{oc\_array}}$ and V_{oc} by (10) as presented in [30], and go directly at $0.8V_{\mathrm{oc\_array}}$ where MPP is expected.

$$V_{\mathrm{oc\_array}} = V_{\mathrm{oc\_array},u} + aV_tN_s \ln\left(\frac{G_1}{G_{\mathrm{STC}}}\right)$$
$$V_{\mathrm{oc}} = V_{\mathrm{oc\_array}}/N_s \tag{10}$$

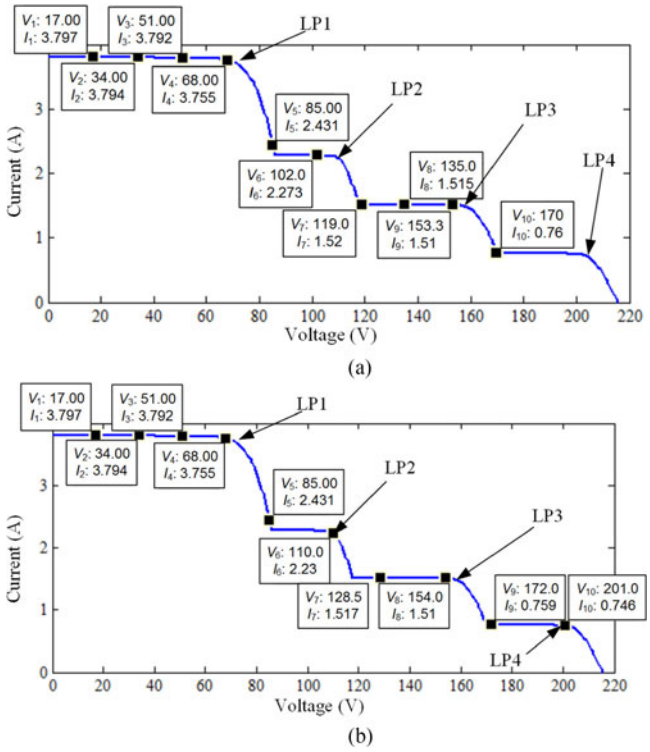

Fig. 5. (a) Predicted points by 0.8Voc model (b) predicted points by EA-P&O.

Then, it initiates P&O under flag 0 and tracks the MPP precisely along with minimizing perturbation size. To notify uniform irradiance condition, a variable named 'cond' is assigned as 0. On the contrary, if it is a case of partial shading then variable 'cond' is assigned as '1' and EA-P&O initiate flag 2 (in Fig. 2) where it performs global peak searching under partial shading.

C. Scanning Under Partial Shading

Under partial shading, the local peaks occur at some specific points. According to $0.8V_{\rm oc}$ model [20], [21] local peaks are expected at the vicinity of the multiples of $0.8V_{\rm oc}$. Thus, scanning the voltages located at multiples of $0.8V_{\rm oc}$ and find the global peak by comparing power is very straight forward. However, it is presented in [32] that when shading level increased along with the number of modules in series, the local peak's positions shifted towards right on the voltage span and the deviation from the multiples of $0.8V_{\rm oc}$ is significant. Thus, to improve the accuracy, it is important to right shift the predicted points along with the increase of the shading level. So, an improved scanning technique is developed and integrated with EA-P&O.

To describe the procedure, the curve presented in the Fig. 5 is considered. The number of modules in series is 10 and these are irradiated by 1000, 600, 400 and 200 W/m^2. The number of modules under each irradiance levels are 3, 3, 2 and 2 respectively. In Fig. 5(a), points scanned by the $0.8V_{\rm oc}$ model is presented. It can be seen if the points according to the $0.8V_{\rm oc}$ model is scanned, the point I_4 is at the LP1. However, the I_6 is not coinciding with the LP2. Although I_9 found the LP3, but LP4 is remain completely un-scanned. This is happening due to the right shifting of the peaks.

In Fig. 5(b), scanning of the EA-P&O is illustrated. EA-P&O starts with scanning the $0.8V_{\rm oc}$ points by assigning $[V_1, V_2 \ldots..V_{Ns}] = [0.8 \times 1 \times V_{oc,}\, 0.8 \times 2 \times V_{oc}.....0.8 \times N_s \times V_{\rm oc}]$ initially. The first scanned point $(V_1,\, I_1)$ is near to the short circuit current. The recoded current is used to calculate the G at the first stair of the current using (9) which is 1000 W/m^2. Then, it scans point V_2 and records current I_2. If G is calculated using (9) at I_2, then the irradiance level is found almost near (difference is less than 50) to the calculated G at I_1. Same observation goes for I_3 and I_4.

However, when $(V_5,\, I_5)$ is scanned and G is calculated as $(2.43/3.8 = 639.5$ W/m$^2)$, EA-P&O realize that current level falls to the second stair. As a consequence, the rest of the predicted peak points needs to be shifted right. Modifying the proposition in [32], local peak position can be calculated considering right shifting phenomenon as follows.

$$V_n = \left[0.8 + (0.97 - 0.8) \times \frac{1}{900} \times \left(\frac{I_1}{I_{\rm sc\_STC}} - \frac{I_{n-1}}{I_{\rm sc\_STC}}\right) \times 1000\right] \times n \times V_{\rm oc} \tag{11}$$

According to the (11) new predicted positions are

$$V_6 = \left[0.8 + (0.97 - 0.8) \times \frac{1}{900} \times \left(\frac{I_1}{I_{\rm sc\_STC}} - \frac{I_{6-1}}{I_{\rm sc\_STC}}\right) \times 1000\right] \times 6 \times V_{\rm oc}$$

$$V_6 = \left[0.8 + (0.97 - 0.8) \times \frac{1}{900} \times \left(\frac{3.797}{3.8} - \frac{2.43}{3.8}\right) \times 1000\right] \times 6 \times 21.1 = 109.88$$

Thus, the V_6 is shifted to 110 V which is at the LP2 precisely. Due to the right shifting V_7 is also shifted to 128.5 V instead of 119 V ($0.8V_{\rm oc}$ model). Here, EA-P&O again sense a change of irradiance level and shift the rest of the peaks. According to (11),

$$V_8 = \left[0.8 + (0.97 - 0.8) \times \frac{1}{900} \times \left(\frac{I_1}{I_{\rm sc\_STC}} - \frac{I_{8-1}}{I_{\rm sc\_STC}}\right) \times 1000\right] \times 8 \times V_{\rm oc}$$

$$V_8 = \left[0.8 + (0.97 - 0.8) \times \frac{1}{900} \times \left(\frac{3.797}{3.8} - \frac{1.517}{3.8}\right) \times 1000\right] \times 8 \times 21.1 = 154.1$$

As a result, V_8 is coinciding with the LP3 accurately. The similar phenomenon will again take place when V_9 is scanned at 172 V and shift the V_{10} to 200 V. That is the actual place of LP4 as marked on Fig. 5 (b). The conclusion can be drawn as if the right shifting mechanism is implemented, the prediction regarding the local peaks position gets more accurate. After scanning all the correctly predicted peaks the scanned power will be compared. Based on the values, the highest power providing position will be considered as the global peak.

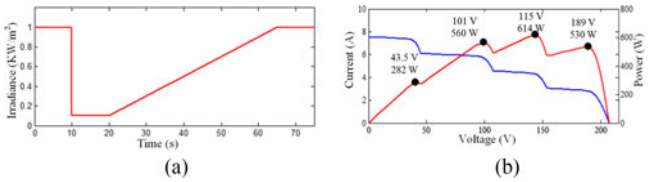

Fig. 6. (a) Variation of irradiance vs. time (b) $P-V$ (red) and $I-V$ (blue) curve under partial shading.

IV. Results and Discussions

The implementation of EA-P&O follows the same Simulink and hardware setup presented in [19]. The simulation adopts the two-diode model configuration. The value of T and G is fed into the simulator and the PV current is delivered to the converter. The buck-boost dc to dc converter is used to convert the output voltage of the MPPT to the load voltage. The converter is designed to operate in the continuous inductor current mode, with the following specifications: switching frequency $(f) =$ 50 kHz, inductor $(L) = 1$ mH and capacitor $C_1 = 470$ μF and $C_2 = 220$ μF.

A. Simulation Results

To verify the working principles of the EA-P&O, a set of tests is designed that comprises of a sudden irradiance change, fast-gradual change with gradient 20 W/m^2/s and a partial shading. The test is implemented on a PV array consist of 10 modules (MSX 60) in a string. Two similar string are connected in parallel. Fig. 6 represents the variation of G for a duration of 75 s. In the beginning, $G = 1000$ W/m^2 and continued for 10 s. Afterwards it falls to 100 W/m^2 and persist for another 10 s. Then G starts increasing following a ramp of gradient 20 W/m^2/s and reached at 1000 W/m^2 at 65 s. After that level, it stays constant at 1000 W/m^2 for another 10 s. immediately after 75 s, the partial shading takes place.

In Fig. 6 (b), the partial shading curve is presented. The PV array is shaded with 4 different levels of G (1000, 800 600 & 400 W/m^2) that manifests the four peaks on the curve. The partial shading continues for 15 s.

In Fig. 7, $V_{\rm PV}$, $I_{\rm PV}$ and $P_{\rm PV}$ depicts the tracking profile of EA-P&O. Some parts of the curves are enlarged to clarify the behavior of the algorithm at the transients. It can be seen in Image 1, that initially EA-P&O starts with large perturbation size $(0.02 \times V_{\rm oc\_array})$. The moment it reaches the MPP and start oscillating, EA-P&O detects it and start reducing the perturbation size (ΔV). Consequently, EA-P&O settles at the MPPT with minimum perturbation size of $0.005 \times V_{\rm oc\_array}$ $(0.005 \times 210 = 1$ V) at 169 V. Following that, a voltage boundary is imposed to restrict the operating point from being diverged.

EA-P&O keeps on tracking the MPP for 10 s and then G falls to 100 W/m^2. This large variation in G induce large deviation in normalized power. Thus $(\Delta P/P)$ is obviously greater than the 0.1. Thus, large power deviation checking condition is satisfied and partial shading occurrence checking is initiated under flag 1. As the mechanism described above, the EA-P&O scans two points on the curve $0.8V_{\rm oc\_array}$ (165.7) V, and $0.8V_{\rm oc}$ (15.87) V. Voltage and the current during this scan can be seen in image 2 and 3 respectively where x is the time and y is the voltage and current in image 2 and 3 respectively. It is noticeable that, another voltage point at (103.3 V) is also scanned while going

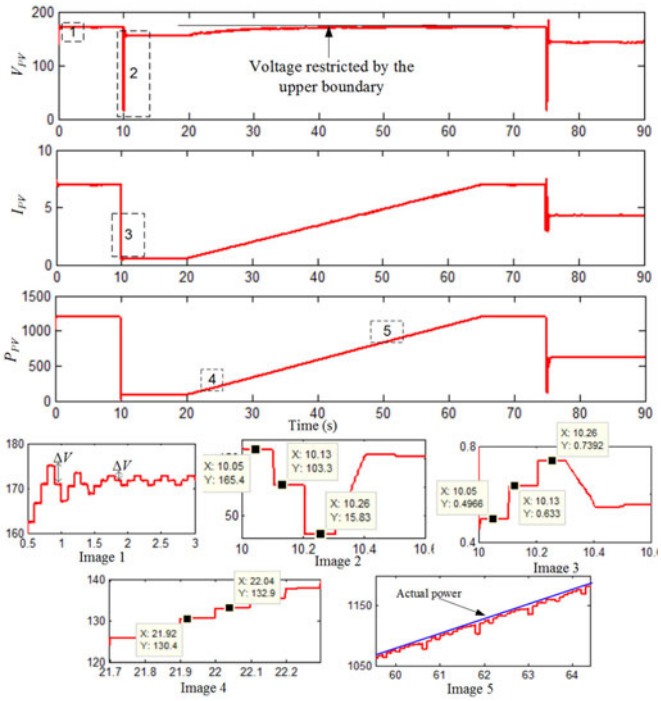

Fig. 7. Tracking profile of EA-P&O.

down from 165.7 V to 15.87 V. This additional voltage scanning is done to provide PI controller sufficient time to go down from 165.7 V to 15.87 V. However, information at 103.3 V is neither recorded nor used in any calculation.

In image 3 of Fig. 7, the recorded current can be found as 0.5 A and 0.74 A at $0.8V_{\rm oc\_array}$ and $0.8V_{\rm oc}$ respectively. During initialization, EA-P&O got the $I_{\rm SC}$ as 3.8 A and $I_{\rm MPP}$ as 3.5 A for MSX 60 modules as an input from datasheet. As there are two strings of module used in this test, thus I_{sc} is 7.6 A and $I_{\rm MPP}$ is 7 A. After scanning the two points, EA-P&O deduce the valued of G_1 *and* G_2 by (8) and (9) respectively as $(0.5/7 \times 100 = 71.4$ W/m$^2)$ and $(0.74/7.6 \times 1000 = 97.36$ W/m$^2)$. Difference between these two-calculated values of G is approximately 25 W/m^2. As the discrepancy is below than 50, EA-P&O will decide that the power change is due to the variation of G not partial shading. After acknowledging the fact that the irradiance level is changed, EA-P&O will recalculate the new $V_{\rm oc\_array}$ and $V_{\rm oc}$ by the (10).

$$V_{\rm oc\_array} = 211 + 1 \times 0.7 \times 10 \ln\left(\frac{97.4}{1000}\right) = 194.69$$

$$V_{\rm oc} = 194.69/10 = 19.47$$

Thus, the newly calculated value of $V_{\rm oc\_array}$ for the G $(100\,{\rm W/m^2})$ is 194.69 V. Afterwards the EA-P&O goes straight back to track the MPP at $(194.69 \times 0.8 = 155.75)$ V and start tracking the MPP at 156 V. In absence of such intelligent mechanism, usual MPPT scheme will consider it as a partial shading case and initiate a global peak searching unnecessarily.

After 20 s, G starts ascending with a gradient 20 W/m^2/s. It can be seen from the $P_{\rm PV}$ curve in Fig. 7 that the EA-P&O is following the MPP trail quiet perfectly instead of being diverged like conventional P&O. Two particular section from the $P_{\rm PV}$ is enlarged in Image 4 and 5 to have a better clarification. Accord-

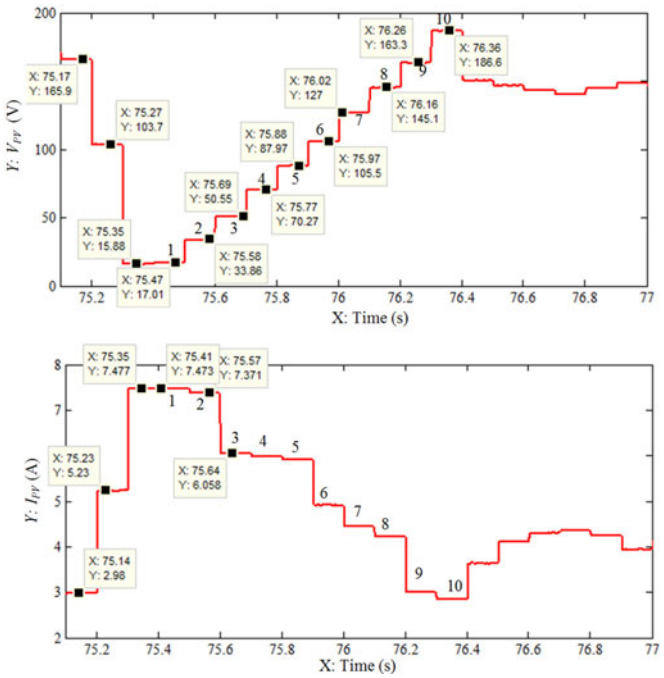

Fig. 8. EA-P&O tracking under partial shading.

ing to (7), when ΔG is 20 W/m^2 then the $\Delta P/P$ is expected to be 0.02. The evidence of that can be seen in the Image 4. In two consecutive samples of power is shown where P_1 and P_2 is 130.4 and 132.9 respectively. Thus, it is calculated as

$$\frac{\Delta P}{P} = \frac{P_2 - P_1}{P_1} = \frac{132.9 - 130.4}{130.4} = 0.019 \approx 0.02$$

As $\Delta P/P$ is greater than the 0.01 but less than 0.1, operating point will be restricted by the voltage boundary. It can be seen from the $V_{\rm PV}$ that the voltage is increasing and reached upper boundary within few seconds. Then the voltage is restricted by the boundary limit and forced to stick near to the MPP. Thus, the divergence problem is avoided successfully. However, it is acknowledged that the tracked voltage is not exactly on the MPP, rather it stays close to the MPP. It can be seen from the Image 5 that the actual power is slightly higher than the tracked power. Nevertheless, the difference is insignificant and the efficiency remains around 99.5%.

Followed by the gradual change of G after 75 s, a partial shading takes place. The transient tracking of EA-P&O under partial shading is illustrated in Fig. 8 from 75 s to 77 s. In can be seen from the $V_{\rm PV}$ that, due to the large drop in power, EA-P&O initiate the partial shading checking by scanning the $0.8V_{\rm oc\_array}$ (165.91 V) and $0.8V_{\rm oc}$ (15.88 V). The corresponding current at $0.8V_{\rm oc\_array}$ is 2.98 A and $0.8V_{\rm oc}$ is 7.477 A, can be found from $I_{\rm PV}$. Thus, the EA-P&O calculated the G_1 and G_2 at $0.8V_{\rm oc\_array}$ as $(2.98/7 \times 1000) = 425\,{\rm W/m^2}$ and at $0.8V_{\rm oc}$ is $(7.477/7.6 \times 1000) = 983\,{\rm W/m^2}$. The difference between the values of G at these two points is 558 W/m^2 (more than 50). As a consequence, EA-P&O decides that partial shading occurs and initiate searching under partial shading.

EA-P&O initiates searching according to the $0.8V_{\rm oc}$ model. Following that model EA-P&O is supposed to scan the 10 points 16.88, 33.76, 50.64, 67.52, 84.42, 101.28, 118.16, 135.04, 151.92 and 168.81 V. The $V_{\rm PV}$ curve in Fig. 8 suggests that EA-P&O scans the first three points accurately, however the fourth point is shifted to 70.27 V instead of 67.52 V. It manifests that the right shifting of the peaks takes place.

To comprehend the procedure, the current notations on $I_{\rm PV}$ curve should be considered. It can be clearly seen that current at sample 1 and 2 is almost at the same level while it drops at the sample 3. After scanning the 3rd sample, EA-P&O recognize that, the current falls from the first stair to second stair. As a consequence, EA-P&O shift rest of the peaks towards right following the relation in (11)

$$V_n = \left[0.8 + (0.97 - 0.8) \times \left(\frac{1}{900}\right) \times \left(\frac{I_1}{I_{sc}} - \frac{I_{n-1}}{I_{sc}}\right) \times 1000\right] \times V_{\rm oc} \times n$$

$$V_4 = \left[0.8 + (0.97 - 0.8) \times \left(\frac{1}{900}\right) \times \left(\frac{7.371 - 6.058}{7.6}\right) \times 1000\right] \times 21.1 \times 4$$

$$V_4 = 70.28$$

Similarly, V_5, $V_6 \ldots\ldots\ldots V_{10}$ will be recalculated as 87.96, 105.55, 123.14, 140.74, 158.33, 175.92 V. A closer look on the $V_{\rm PV}$ curve suggest that EA-P&O is scanning the newly calculated peak for V_4, V_5 and V_6. However, it is shifted again for the V_7 from 123.14 V to 127 V. The reason can be comprehended from the $I_{\rm PV}$ curve once again. For the sample 3, 4 and 5 currents are almost at the same level but it sharply falls at sample 6. Thus, it shifts the V_7, V_8, V_9 and V_{10} following the same procedure as stated above. In $I_{\rm PV}$ curve another sharp fall can be seen at the sample 9. As a follow-through, EA-P&O realized current has fallen again from the stair 3 to stair 4 and shift the V_{10} accordingly.

Due to that right shifting, the scanned peak gets closer to the actual local peaks as marked in the PS curve Fig. 6(b). Thus, the inclusion of this intelligent right shifting method, EA-P&O provides better accuracy to locate the actual global peak under partial shading and confirm the maximum power extraction under partial shading.

B. Comparisons With Other MPPT

The performance of the proposed EA-P&O is evaluated against four recent MPPT techniques, namely the modified incremental conductance (MIC) [33], artificial bee colony (ABC) [5], cuckoo search (CS) [8] and a hybrid scheme that combines P&O with the ant colony optimization (ACO-P&O) [4]. These techniques are deliberately chosen to compare the relative effectiveness of EA-P&O: the MIC represents the conventional MPPT with an adaptive feature; the ABC and CS are the metaheuristic types, while the ACO-P&O represents the hybrid MPPT schemes. To generate the $I-V$ and $P-V$ curve, a 10×5 S-P array is constructed using the MSX60 modules. All these algorithms are tested with three partial shading curves with diversified MPP positions, as presented in Fig. 9. For partial shading pattern 1 (PS1), there are three peaks; the global peak $(G_{\rm MPP1})$ is at the middle section of the voltage -axis. For shading pattern 2 (PS2), the $G_{\rm MPP2}$ is at the extreme left; it has a total of four peaks. Finally, the $G_{\rm MPP3}$ lies on the extreme right of the partial shading (PS3) curve. It contains five peaks. For

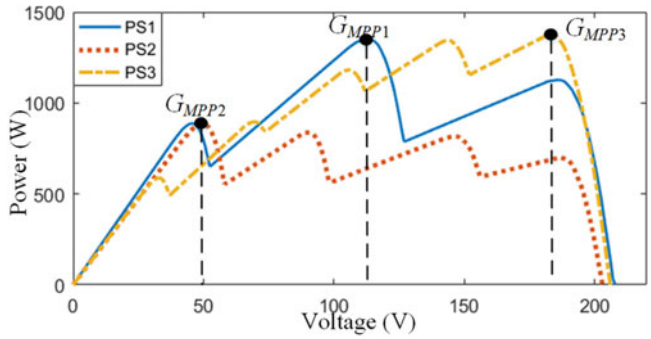

Fig. 9. Partial shading curves for performance evaluation of EA-P&O against four different MPP techniques.

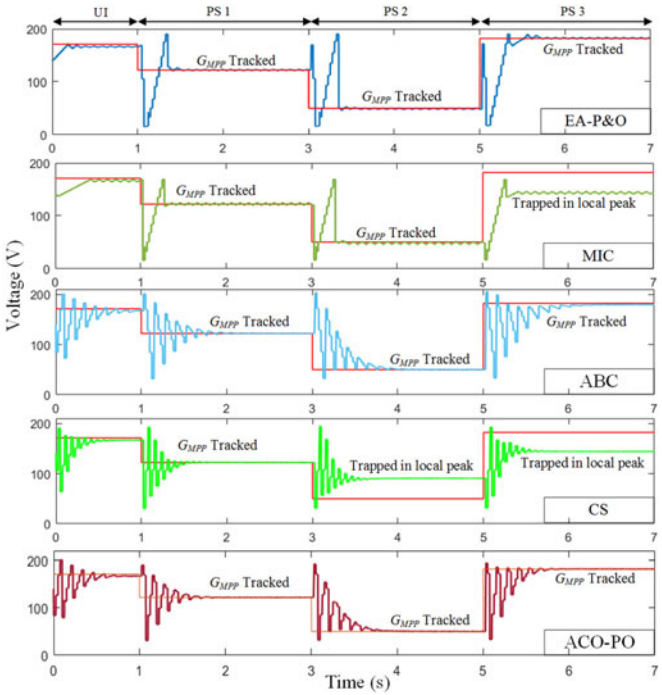

Fig. 10. Voltage profile for EA-P&O, MIC, ABC, CS & ACO-P&O.

the test sequence, the uniform irradiance is imposed for the first 1 s; then three partial shading curves are applied successively for 2 s each.

The voltage tracking profiles of the EA-P&O, MIC, ABC, CS and ACO-P&O are presented in Fig. 10. Initially all algorithms track the MPP under uniform irradiance correctly. After the lapse of 1 s, PS1 is imposed. As can be seen, the proposed method (EA-P&O) converges to G_{MPP1} (122 V) after 250 ms. Since, there are 10 modules in series, it requires 10 samples to track G_{MPP1}. The MIC also reaches to G_{MPP1} at about the same time. On the other hand, the ABC requires 30 samples (750 ms) to converge, while the ACO-P&O tracks the G_{MPP1} within 22 sample (550 ms). Furthermore, ABC and ACO-P&O exhibit much larger transient fluctuation due to the random exploration performed by the search agents. In the case of CS, it is faster than ABC and ACO-P&O. This is because CS incorporates the Levy flight for faster convergence compared to other metaheuristic algorithms. However, expectedly, it is slower than EA-P&O and MIC.

For PS2, all the algorithm successfully tracks the global peak, except for CS. As mentioned earlier, due to Levy flights, the search agents in CS jumps faster towards the local best positions. Since G_{MPP2} lies at an extreme left position, the CS agents occasionally miss the global peak. In terms of tracking speed, EA-P&O and MIC track G_{MPP2} within 10 samples. The. ABC and ACO-P&O is significantly slower, i.e., 32 and 24 samples, respectively. For PS3, it is interesting to note that MIC misses the global peak (G_{MPP3}). This can be attributed to the fact that the MIC is based on the $0.8V_{\mathrm{oc}}$ model, which only scans the integer multiples of $0.8 \times V_{\mathrm{oc}}$. Since G_{MPP3} is located at the extreme right of the voltage span (182 V), it is beyond the range of $0.8V_{\mathrm{oc}}$ model $(10 \times 0.8V_{\mathrm{oc}} = 168.8$ V). Consequently, it gets trapped at a local peak (140 V). This problem is not experienced by the EA-P&O because it incorporates the right shifting scheme, as explained in Section III (C). Similar to MIC, CS also gets trapped at the same local peak (140 V). On the other hand, ABC and ACO-P&O tracks G_{MPP3} successfully, albeit slower than EA-P&O.

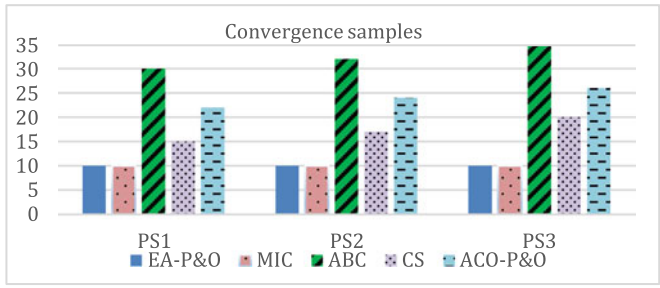

Fig. 11. Convergence samples of all five MPPT algorithms under partial shading.

TABLE III
COMPARISON TABLE BETWEEN EA-P&O AND OTHER MPPT TECHNIQUES

Parameters	EA-P&O	MIC	ABC	ACO-P&O	CS
G_{MPP} tracking guaranteed?	Yes	No	Yes	Yes	No
Convergence samples (ms)	10	10	30–35	22–26	15–20
Convergence time (ms)	250	250	625–750	750–875	375–500
Complexity	Med	Med	High	Med	High
Tuning parameters	None	None	2	1	2
Reliability	High	Med	High	High	Med
System dependency?	Yes	No	No	No	Yes
Load dependency?	No	Yes	Yes	Yes	No

The number of samples required for convergence is shown in Fig. 11. Clearly, other than MIC, the proposed method outperforms other competing algorithms by a significant margin. Although, the MIC is equally fast, it does not guarantee that the G_{MPP} can be tracked under certain partial shading curve, as proven by its inability to detect G_{MPP3}.

Other features of the compared methods are summarized in Table III. The metaheuristic techniques like ABC, ACO-P&O always need to make a trade-off between number of search agents and convergence probability. In order to guarantee convergence under partial shading, usually high number of agents (5 or 6) are initialized in ABC and ACO-P&O. Although higher

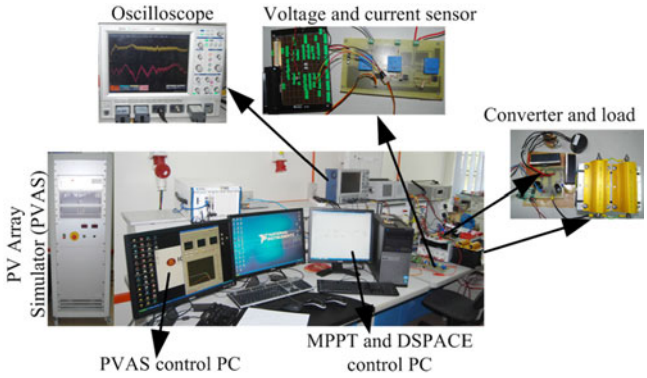

Fig. 12. Hardware setup to implement EA-P&O.

number of agents improves the probability of global peak detection, the tracking speed is compromised. On the contrary, CS uses only 3 agents, which increase the speed. However, it does not guarantee $G_{\rm MPP}$ tracking, as demonstrated by its failure to track $G_{\rm MPP2}$.

The ABC and CS require two parameters to be tuned for optimized operation, while ACO-P&O requires one. On the other hand, for both EA-P&O and MIC, parameter tuning is not needed, which gives them programming advantages. Another point to be noted is that, EA-P&O is a voltage based MPPT algorithm; thus, it is dependent on the STC data provided by the manufacturers. Due to aging of the module, the module parameters values, i.e., $V_{\rm OC}$, $I_{\rm SC}$, $I_{\rm MPP}$ (at STC) continuously (but slowly) degrade with time. Therefore, it is necessary to adjust the STC values periodically. CS also have similar limitation. However, being a voltage based algorithm, EA-P&O and CS do not suffer from load variation. As a result, they exhibit less transient fluctuations during tracking. On the contrary, the MIC, ABS and ACO-P&O are based on direct duty cycle MPPT. This makes them independent of parameters variations due to aging. Despite such advantage, duty cycle based algorithm suffers from the effect of constant load variations, as highlighted by [33].

Furthermore, the EA-P&O still retains comparatively simple structure. Compared to the metaheuristic techniques, its implementation is much simpler. In addition, it does not require any additional sensors like temperature and irradiance sensors.

C. Partial Shading Test on Hardware

To verify the performance of EA-P&O in hardware, Dspace platform (DS1104 board) in conjunction with buck-boost converter is implemented. The hardware setup is presented in Fig. 12. For hardware verification, three different partial shading curves are imposed on the PV array as presented in Fig. 13. Hardware implementation is based on a smaller prototype comprises four modules in series. Thus, maximum possible local peaks on the $P-V$ curve is 4. The test begins with the uniform irradiance. The first pattern represents uniform irradiance, thus contains a single peak at 68 V.

Afterwards, uniform irradiance is replaced by the partial shading pattern in curve 2. The global peak lies at 72 V. Then again, the uniform irradiance is restored back to clarify the transition from the partial shading to uniform irradiance. Following that, partial shading takes place again through curve 3. It also presents 4 peaks, however global peak is shifted to 52 V.

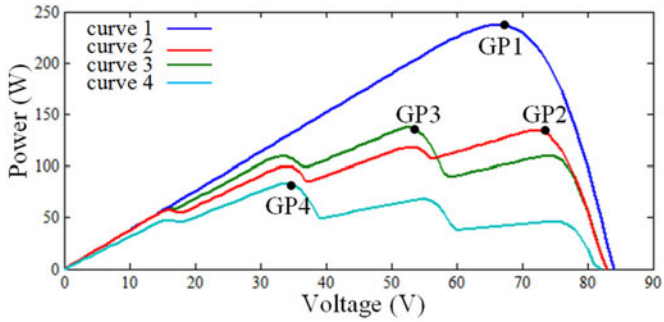

Fig. 13. Partial shading patterns applied in the hardware.

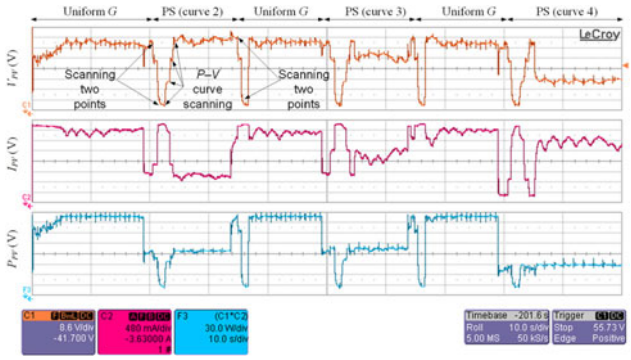

Fig. 14. Tracking profile of EA-P&O from oscilloscope.

Following that partial shading pattern, uniform irradiance of curve 1 is reinstated again. Finally, another partial shading takes place through curve 4 where global peak is located at 34 V.

The oscillogram of the EA-P&O tracking depicted in Fig. 14. It can be seen from the $V_{\rm PV}$ that at the beginning EA-P&O tracks the MPP and minimize the steady state oscillation. When partial shading takes place by curve 2, EA-P&O initiates partial shading occurrence checking by scanning two predetermined points. After the checking, EA-P&O decides successfully that partial shading occurs and goes for the $P-V$ curve scanning. It scans the four points on the curve and finds the global peak at 72 V by comparing the respective power at these points. Thus, GP2 is tracked successfully.

Following that period, uniform irradiance is restored and EA-P&O sense a large change in power. Thus, it starts the partial shading occurrence checking again by scanning two points on the curve. EA-P&O recognize successfully that the PV module is under uniform irradiance now, thus by updating $V_{\rm oc\_array}$ and goes to that position directly. The similar phenomenon can be seen in the case of curve 3 and 4. In both cases, EA-P&O successfully locate the global peak at 52 V and 33 V.

V. Conclusion

In this paper, a new MPPT scheme is proposed to mitigate all the limitations of conventional P&O simultaneously. The presented scheme is able to diminish the power loss due to steady state oscillation, divergence problem and partial shading. Besides, it offers continuous updating of open circuit voltage without any irradiance and temperature sensors. In addition to that, this scheme can identify the occurrence of partial shading precisely which saves many unnecessary global peak scanning and power loss. Rigorous simulation and hardware results clarify the

behavior of the algorithm which ensure overall efficiency around 99% under any environmental variations. Thus, this algorithm can be an optimum solution for all the environmental challenges that MPPT may face during practical operations. However, it has to be noted that, the algorithm is dependent on several initial parameters which are required to be chosen carefully and provided during initialization stage of the controller. Besides, the $I-V$ and $P-V$ characteristics used to develop this scheme are adopted from mono and polycrystalline based PV modules. Thus, in thin film modules, EA-P&O is not applicable.

REFERENCES

[1] H. Renaudineau *et al.*, "A PSO-based global MPPT technique for distributed PV power generation," *IEEE Trans. Ind. Electron.*, vol. 62, no. 2, pp. 1047–1058, Feb. 2015.

[2] M. Seyedmahmoudian *et al.*, "Simulation and hardware implementation of new maximum power point tracking technique for partially shaded PV system using hybrid DEPSO method," *IEEE Trans. Sustain. Energy*, vol. 6, no. 3, pp. 850–862, Jul. 2015.

[3] K. Punitha, D. Devaraj, and S. Sakthivel, "Artificial neural network based modified incremental conductance algorithm for maximum power point tracking in photovoltaic system under partial shading conditions," *Energy*, vol. 62, pp. 330–340, 2013.

[4] K. Sundareswaran, V. Vigneshkumar, P. Sankar, S. P. Simon, P. S. R. Nayak, and S. Palani, "Development of an improved P&O algorithm assisted through a colony of foraging ants for MPPT in PV system," *IEEE Trans. Ind. Informat.*, vol. 12, no. 1, pp. 187–200, Feb. 2016.

[5] K. Sundareswaran, P. Sankar, P. S. R. Nayak, S. P. Simon, and S. Palani, "Enhanced energy output from a PV system under partial shaded conditions through artificial bee colony," *IEEE Trans. Sustain. Energy*, vol. 6, no. 1, pp. 198–209, Jan. 2015.

[6] S. Mohanty, B. Subudhi, and P. K. Ray, "A new MPPT design using grey wolf optimization technique for photovoltaic system under partial shading conditions," *IEEE Trans. Sustain. Energy*, vol. 7, no. 1, pp. 181–188, Jan. 2016.

[7] D. Teshome, C. H. Lee, Y. W. Lin, and K. L. Lian, "A modified firefly algorithm for photovoltaic maximum power point tracking control under partial shading," *IEEE J. Emerg. Sel. Topics Power Electron.*, vol. 5, no. 2, pp. 661–671, Jun. 2017.

[8] J. Ahmed and Z. Salam, "A maximum power point tracking (MPPT) for PV system using cuckoo search with partial shading capability," *Appl. Energy*, vol. 119, pp. 118–130, Apr. 2014.

[9] J. Ahmed and Z. Salam, "A critical evaluation on maximum power point tracking methods for partial shading in PV systems," *Renewable Sustain. Energy Rev.*, vol. 47, pp. 933–953, Jul. 2015.

[10] K. Ishaque and Z. Salam, "A review of maximum power point tracking techniques of PV system for uniform insolation and partial shading condition," *Renewable Sustain. Energy Rev.*, vol. 19, pp. 475–488, Mar. 2013.

[11] S. K. Kollimalla and M. K. Mishra, "Variable perturbation size adaptive P&O MPPT algorithm for sudden changes in irradiance," *IEEE Trans. Sustain. Energy*, vol. 5, no. 3, pp. 718–728, Jul. 2014.

[12] S. K. Kollimalla and M. K. Mishra, "A novel adaptive P&O MPPT algorithm considering sudden changes in the irradiance," *IEEE Trans. Energy Convers.*, vol. 29, no. 3, pp. 602–610, Sep. 2014.

[13] F. Zhang, K. Thanapalan, A. Procter, S. Carr, and J. Maddy, "Adaptive hybrid maximum power point tracking method for a photovoltaic system," *IEEE Trans. Energy Convers.*, vol. 28, no. 2, pp. 353–360, Jun. 2013.

[14] F. Paz and M. Ordonez, "Zero oscillation and irradiance slope tracking for photovoltaic MPPT," *IEEE Trans. Ind. Electron.*, vol. 61, no. 11, pp. 6138–6147, Nov. 2014.

[15] M. Killi and S. Samanta, "Modified perturb and observe MPPT algorithm for drift avoidance in photovoltaic systems," *IEEE Trans. Ind. Electron.*, vol. 62, no. 9, pp. 5549–5559, Sep. 2015.

[16] T. Bennett, A. Zilouchian, and R. Messenger, "A proposed maximum power point tracking algorithm based on a new testing standard," *Sol. Energy*, vol. 89, pp. 23–41, 2013.

[17] A. Pandey, N. Dasgupta, and A. K. Mukerjee, "High-performance algorithms for drift avoidance and fast tracking in solar MPPT system," *IEEE Trans. Energy Convers.*, vol. 23, no. 2, pp. 681–689, Jun. 2008.

[18] E. Mamarelis, G. Petrone, and G. Spagnuolo, "A two-steps algorithm improving the P& O steady state MPPT efficiency," *Appl. Energy*, vol. 113, pp. 414–421, Jan. 2014.

[19] J. Ahmed and Z. Salam, "A modified P&O maximum power point tracking method with reduced steady-state oscillation and improved tracking efficiency," *IEEE Trans. Sustain. Energy*, vol. 7, no. 4, pp. 1506–1515, Oct. 2016.

[20] H. Patel and V. Agarwal, "Maximum power point tracking scheme for PV systems operating under partially shaded conditions," *IEEE Trans. Ind. Electron.*, vol. 55, no. 4, pp. 1689–1698, Apr. 2008.

[21] A. Kouchaki, H. Iman-Eini, and B. Asaei, "A new maximum power point tracking strategy for PV arrays under uniform and non-uniform insolation conditions," *Sol. Energy*, vol. 91, pp. 221–232, May 2013.

[22] C. Kai, T. Shulin, C. Yuhua, and B. Libing, "An improved MPPT controller for photovoltaic system under partial shading condition," *IEEE Trans. Sustain. Energy*, vol. 5, no. 3, pp. 978–985, Jul. 2014.

[23] C. Manickam, G. P. Raman, G. R. Raman, S. I. Ganesan, and N. Chilakapati, "Fireworks enriched P&O algorithm for GMPPT and detection of partial shading in PV systems," *IEEE Trans. Power Electron.*, vol. 32, no. 6, pp. 4432–4443, Jun. 2017.

[24] C. Manickam, G. R. Raman, G. P. Raman, S. I. Ganesan, and C. Nagamani, "A hybrid algorithm for tracking of GMPP based on P&O and PSO with reduced power oscillation in string inverters," *IEEE Trans. Ind. Electron.*, vol. 63, no. 10, pp. 6097–6106, Oct. 2016.

[25] K. Sundareswaran and S. Palani, "Application of a combined particle swarm optimization and perturb and observe method for MPPT in PV systems under partial shading conditions," *Renewable Energy*, vol. 75, pp. 308–317, 2015.

[26] S. Mohanty, B. Subudhi, and P. K. Ray, "A grey wolf-assisted perturb & observe MPPT algorithm for a PV system," *IEEE Trans. Energy Convers.*, vol. 32, no. 1, pp. 340–347, Mar. 2017.

[27] K. Ishaque, Z. Salam, and H. Taheri, "Simple, fast and accurate two-diode model for photovoltaic modules," *Sol. Energy Mater. Sol. Cells*, vol. 95, no. 2, pp. 586–594, 2011.

[28] M. G. Villalva and J. R. Gazoli, "Comprehensive approach to modeling and simulation of photovoltaic arrays," *IEEE Trans. Power Electron.*, vol. 24, no. 5, pp. 1198–1208, May 2009.

[29] J. Ahmed and Z. Salam, "An improved perturb and observe (P&O) maximum power point tracking (MPPT) algorithm for higher efficiency," *Appl. Energy*, vol. 150, pp. 97–108, 2015.

[30] J. Ahmed and Z. Salam, "An accurate method for MPPT to detect the partial shading occurrence in a PV system," *IEEE Trans. Ind. Informat.*, vol. 13, no. 5, pp. 2151–2161, Oct. 2017.

[31] Y.-H. Liu, J.-H. Chen, and J.-W. Huang, "A review of maximum power point tracking techniques for use in partially shaded conditions," *Renewable Sustain. Energy Rev.*, vol. 41, pp. 436–453, Jan. 2015.

[32] J. Ahmed and Z. Salam, "An improved method to predict the position of maximum power point during partial shading for PV arrays," *IEEE Trans. Ind. Informat.*, vol. 11, no. 6, pp. 1378–1387, Dec. 2015.

[33] K. S. Tey and S. Mekhilef, "Modified incremental conductance algorithm for photovoltaic system under partial shading conditions and load variation," *IEEE Trans. Ind. Electron.*, vol. 61, no. 10, pp. 5384–5392, Oct. 2014.

Jubaer Ahmed (M'16) received the B.Sc. degree in electrical and electronics engineering from the Bangladesh University of Engineering and Technology, Dhaka, Bangladesh, in 2012, and the Ph.D. degree from the Universiti Teknologi Malaysia, Johor, Malaysia, in 2016. He is currently a Lecturer with the Swinburne University of Technology Sarawak, Kuching, Malaysia. His research interests include photovoltaic modeling and control, energy conversion from renewable sources, and power electronics.

Zainal Salam (M'90) received the B.Sc. degree from the University of California, Chico, Chico, CA, USA, in 1985, the M.E.E. degree from Universiti Teknologi Malaysia (UTM), Kuala Lumpur, Malaysia, in 1989, and the Ph.D. degree from the University of Birmingham, Birmingham, U.K., in 1997. He was a Lecturer with UTM for 30 years and is currently a Professor in power electronics. He is currently the Director of the Inverter Quality Control Centre, UTM, and is responsible for testing photovoltaic inverters. His research interests include power electronics, renewable energy, power systems, and machine control. He was the Editor for the IEEE TRANSACTION SUSTAINABLE ENERGY (2011–2013).